Received: 23 November 2023 | Revised: 02 January 2024 | Accepted: 14 January 2024
DOI: 10.48309/jmpcr.2024.187638
Journal of Medicinal and Pharmaceutical Chemistry Research
SAMI

FULL PAPER

High-performance of fluorine-doped tin oxide immobilized on polyurethane foam composite for crude glycerol to ethyl acetate photoconversion

Sadina Shazwani Mastika[a,*]| Noraini Hamzah[b]| Norazzizi Nordin[c]| Wan Zurina Samad[a]

[a]*Department of Chemistry, Kulliyyah of Science, International Islamic University Malaysia (IIUM), Jalan Sultan Ahmad Shah, Bandar Indera Mahkota, 25200 Kuantan, Pahang, Malaysia*

[b]*School of Chemistry and Environment, Faculty of Applied Sciences, UiTM, 40450 Shah Alam, Selangor, Malaysia*

[c]*School of Chemical Sciences, Universiti Sains Malaysia, 11800 Gelugor, Pulau Pinang, Malaysia*

Photocatalytic conversion of crude glycerol into high-value products offers economic and environmental benefits. However, impurities such as organic and inorganic salts, heavy metals, soap, and matter organic non-glycerol (MONG) can hinder direct conversion. This study investigates the transformation of non-purified crude glycerol into value-added products such as ethyl acetate using a newly developed fluorine-doped tin oxide (FTO) photocatalyst immobilized on polyurethane foam (PU). FTO-PU was synthesized by a simple mixture method, and the FTO cluster was evenly distributed on the PU foam, obstructing intrinsic PU pores and leading to a smaller surface area for FTO-PU than FTO catalysts. Despite the smaller surface area, the FTO-PU catalyst demonstrated exceptional performance, achieving 94% conversion of crude glycerol with 86% selectivity to ethyl acetate, resulting in an 81% yield. The stability and reusability of the FTO-PU catalyst were confirmed over six cycles, demonstrating its potential for efficient crude glycerol conversion and laying the foundation for advanced materials in photocatalytic systems. Critical parameters, including light power, reaction time, crude glycerol concentration, and FTO loading within the PU structure, were optimized, with 2% FTO loading on PU, 70 W light intensity, 60 min reaction time, and 10 wt% crude glycerol concentration identified as optimal conditions. Importantly, this study aligns with Sustainable Development Goal 12, emphasizing sustainable consumption and production patterns. By addressing impurities in crude glycerol and converting it into high-value products, this research contributes to efficient resource management and supports the responsible disposal of waste, aligning with global efforts for a sustainable future.

***Corresponding Author:**
Sadina Shazwani Mastika
Email: sadinamastika@gmail.com
Tel.: + 1152411160

KEYWORDS

Fluorine-doped tin oxide; polyurethane foam; crude glycerol conversion; free radical; surface area.

Introduction

As global energy demand continues to increase, fossil fuels have played a pivotal role in meeting this demand since the inception of the Industrial Revolution. In 2023, fossil fuels, including gasoline, diesel, coal, and natural gas, accounted for a staggering 82% of the world's primary energy consumption, solidifying their status as the predominant

energy source on a global scale [1]. However, at current rates, oil and gas reserves may deplete in about 50 years. From an environmental perspective, the combustion of fossil fuels releases gaseous pollutants, such as greenhouse gasses, which alter the atmospheric composition, resulting in adverse effects on climate and public health. In 2019, fossil fuels were responsible for 74% of greenhouse gas (GHG) emissions in the United States [1].

Approximately 58% of fossil fuels are consumed within the transportation sector, which is an essential component of modern society. To eliminate fossil fuel dependence by 2050, renewable energy generation needs a significant increase, from six to eight times [2]. Therefore, it is crucial to transition from conventional fossil fuels to greener, renewable energy sources to reduce GHG emissions, stabilize the global climate, and improve energy security. These renewable energy sources include solar, wind, hydro, geothermal, and biofuels [3].

Among these options, biofuels stand out as an up-and-coming energy source for the transportation sector. Biofuels represent one of the most potential energy sources in the transportation industry. According to the annual energy outlook of the Energy Information Administration (EIA), biofuel usage is expected to steadily increase by 2050 despite the COVID-19 pandemic. To maintain and increase the biofuel supply by 2050, the EIA plans to continuously expand the percentage of biofuels mixed with the US transportation fuel pool [4].

These environmentally friendly alternatives to diesel can decrease CO_2 emissions by as much as 41%, offer superior engine performance with complete combustion, require no modifications to diesel engines, and come at a lower cost. Among the biofuels, biodiesel production from various sustainable sources, including plant oils, animal fats, and recycled oils, has become the most outstanding and is being focused on its development due to its eco-friendly fuel. Biodiesel is produced through a transesterification reaction in which two distinct phases are formed: an upper phase known as biodiesel (comprising methyl or ethyl esters) and a lower phase referred to as crude glycerol. Transesterification of biodiesel yields a ratio of 3:1 of crude glycerol as a by-product. In 2017, the Organization for Economic Cooperation and Development (OECD) reported that global biodiesel production in the previous year amounted to approximately 36 billion liters and is expected to increase in the following years. Malaysia, the world's second-biggest producer of palm oil, currently implements the B10 biodiesel program with 30% palm oil, scheduled for full implementation by 2025 solely for the transportation sector.

Hence, increasing biodiesel production and its crude glycerol yield can result in the abundance of this source in nature. Furthermore, the purification of crude glycerol has become of interest in many studies because pure glycerol has three reactive hydroxyls that can be transformed into value-added products. However, the high cost of crude glycerol refining seems to be an unappealing option for many biodiesel industry players. The presence of various impurities in crude glycerol necessitates purification processes, which are not only cumbersome and expensive, but also raise environmental concerns because treatment is required before discharge into the atmosphere [5-6].

These impurities encompass alcohol, organic and inorganic salts, heavy metals, water, soap, mono- and di-glyceride residues, organic non-glycerol matter (MONG), fatty acid methyl esters (FAME), fatty acid esters (FAE), free fatty acids (FFA), polyol, and ash. These impurities can significantly impact the properties of crude glycerol and hinder its conversion into value-added products. For example, even at 80% purity, crude glycerol is too damaging for Olechemical refineries to use, as it would harm the expensive pipes and storage equipment [7].

Hence, a purification process is needed to use glycerol for various applications such as value-added chemical, textile, pharmaceutical, and food industries [4]. However, the purification process, which involves filtration, chemical treatment, and vacuum distillation, is expensive, especially for small and medium production plants. The purification cost is inconsistent with its low market value [9]. Therefore, considerable attention has recently been directed toward utilizing crude glycerol or partially treated raw glycerol in producing higher-value products without undergoing purification. This will likely promote integrated biodiesel and chemical production, also known as biorefineries [9,10].

Many methods have been used for conversion, such as biological methods, fermentation, and catalytic converters, which use high temperatures and longer reaction times [11]. For example, using a Cu-Ni catalyst, the study used 250 °C, 40 bar, and 6 hours to convert glycerol to propylene glycol [12] while the biological method of *G. Oxydans* cells immobilized over polyurethane foam can convert crude glycerol to 1,3-dihydroxyacetone for 2-3 days [13]. Therefore, photocatalysis is an alternative to traditional conversion methods that offer several significant advantages, including generating non-toxic products using mild reaction conditions, modest reaction durations, reduced chemical input requirements, and minimal secondary waste generation. This method is appealing due to its capacity to harness solar energy as a sustainable energy source and its efficiency under mild light conditions, reducing pollutant emissions [14].

Incorporating solar energy can contribute to decreasing fossil fuel consumption, thereby aiding in mitigating environmental issues [15]. Furthermore, the utilization of the photocatalytic process offers a promising avenue for obtaining value-added chemicals from glycerol. For example, Rh-TiO_2-based photocatalysts result in over 90% superior selectivity of hydroxyacetaldehyde when irradiated with a 300 W Xe-lamp and for 1 hour [16].

WO_3-based materials photocatalysts have demonstrated remarkable selectivity towards glyceraldehyde (~40%) and glycerol conversion (~75%) under room temperature [17].

However, it is worth noting that while numerous studies have concentrated on pure glycerol conversion, only a limited number have explored the conversion of crude glycerol through photocatalysis. Moreover, to the best of our knowledge, the transformation of crude glycerol into ethyl acetate has not been previously investigated, and this study successfully demonstrates the viability of such conversion. Ethyl acetate is widely employed as a solvent in various chemical reactions within the industrial sector, serving roles such as a binder, extractant, and aromatic raw material [18].

The utilization of ethyl acetate has witnessed consistent growth over the past decades, and this trend is expected to continue in the foreseeable future. Consequently, there is a pressing need to enhance existing ethyl acetate production to meet the rising demand. In light of contemporary regulations imposed by many countries on the release of harmful pollutants during production processes, the recognition of green chemistry products, characterized by their non-toxicity to the environment and living organisms, has become prominent. Therefore, there is an urgent imperative for commonly used solvents to adopt green chemistry principles. Ethyl acetate, distinguished by its low toxicity and biodegradability, has experienced a surge in market demand as a result. Current ethyl acetate production methods include direct esterification, acetaldehyde condensation, ethanol dehydrogenation, and ethylene addition. Direct esterification faced challenges such as equipment corrosion, post-processing complexities, and waste acid pollution [19]. Ethylene addition exhibits high selectivity but lacks efficiency, with conversion rates ranging

from 40% to 50% depending on the catalyst [20].

Ethanol dehydrogenation results in by-products, including other esters, alcohols, aldehydes, and ketones, posing challenges for high-purity ethyl acetate production. In this study, an alternative method was explored, involving the conversion of crude glycerol to ethyl acetate using the FTO-PU catalyst in photocatalysis. FTO has been used extensively in electronic applications as a semiconductor. Recently, it has been used as an active catalyst in biomass conversion to renewable energy due to its unique properties, such as being amphoteric, having high thermal stability, and possessing conducting properties. FTO has previously shown great potential in converting purified glycerol into different chemicals, such as 1,2-propanediol and methanol, via hydrogenolysis (Parr reactor) and sub-critical water methods [21-22]. However, it has a problem with leaching, as FTO catalyst powder could cause colour changes in the product and weight loss of the catalyst when recycled, which can decrease the catalyst recyclability performance. Hence, polymer modification with PU has been proposed to improve the FTO catalyst properties. PU has unique characteristics that can contribute significantly to the photoconversion of crude glycerol.

The attributes of PU's adsorption performance include hydrophobicity and specific surface area. Hydrophobicity is essential for selectively removing organic pollutants and oil. The main component of castor oil, ricinoleic acids, is responsible for the hydrophobicity in a polyurethane/castor oils biocomposite [23].

PU is heterogeneous and porous, absorbing pollutants via its cavities. In addition, its wettability is impacted by structural roughness [24]. Due to its high glass temperature and thermal stability, PU can be utilized at elevated temperatures, as shown in an investigation of PU/castor oils biocomposites that demonstrated usage at temperatures not exceeding 284 ℃. PU is easily and inexpensively regenerated through multiple cycles, as evidenced by an experiment that found no deterioration even after 150 uses due to its inherent elasticity [24].

PU has also been employed as a support material for a heterogeneous catalyst for cyanide degradation in wastewater. Specifically, the S-TiO_2@rGO heterogeneous photocatalyst immobilized on PU foam (PUF) achieved high cyanide degradation and toxicity removal percentages [25]. Furthermore, the use of PU as a supporting material in catalytic systems emphasizes its practicality through the application of the user-friendly "dip-and-play" mode, which involves immersing the composite in the liquid reaction medium at the process's onset and retrieving it at the end without causing the leached-out catalyst [26].

These unique properties of PU foam effectively bypass the extended filtration and centrifugation steps frequently associated with powdered heterogeneous catalysts. In this study, we pioneered the use of PU as a photocatalyst, in conjunction with FTO, to form a composite photocatalyst- a novel approach in catalyst research yet to be explored in crude glycerol photoconversion. Overall, this study aimed to successfully synthesize and characterize an FTO-PU composite photocatalyst that effectively transforms non-purified crude glycerol into ethyl acetate, achieving high conversion rates and product selectivity without encountering leaching issues.

Experimental

Materials

Tin (IV) chloride pentahydrate ($SnCl_4.5H_2O$, >98% purity), ammonium fluoride (NH_4F, >95%), ethanol, and deionized water were used for FTO preparation. Crude glycerol was supplied by Felda Global Ventures (FGV) Holdings Berhad, Gebeng Kuantan, Pahang. Meanwhile, castor oil, ethylene glycol, silicon

oil, and toluene diisocyanate (TDI) were purchased and used for PUF synthesis. All chemicals were used with no further purification.

Photocatalyst Synthesis

To achieve an effective photocatalyst in the form of FTO-PU, it is imperative to establish the stability of the FTO powder catalyst, as it plays a pivotal role in converting crude glycerol.

Synthesis of the FTO catalyst

An amount of $SnCl_4.5H_2O$ was dissolved in 100 ml of ethanol. Continuously stirred and heated for 5 hours until a homogeneous solution of $SnCl_4.5H_2O$ was obtained and was labeled as Mixture A. Mixture B was prepared by dissolving 2.0 g of NH_4F in 5 ml of deionized water in a sealed container. Next, mixture A was continuously stirred in a water bath at 60 °C before adding mixture B. The mixture was heated and stirred at 60 °C overnight for complete mixing. Next, the mixture was dried in an oven at 110 °C to remove solvent and moisture. The resulting powder was ground to a fine and uniform powder before being calcined in a furnace at 450 °C for 3 hours.

PU foam synthesis

Briefly, 10.0 g of castor oil, 3.0 g of ethylene glycol, 0.5 g of distilled water, and 45 µL of silicon oil were mixed and stirred in a beaker until a white cloudy mixture formed. TDI was added to the mixture with the ratio volume of TDI to castor oil being 1:1 and stirred for 1 min. Then, the solution was immediately poured into a plastic cup, allowed to rise, and cured at room temperature for 24 hours.

Synthesis of the FTO-PU foam

The same procedure from synthesizing PU was repeated by adding FTO at mass ratios of 1%, 2%, and 3% before TDI was added. All reagents of PU and FTO should form homogenously when TDI is poured. The percentage of FTO was determined by calculating the FTO weight ratio to the total weight of all PU reagents.

Characterizations

Attenuated total reflectance (ATR)-Fourier transform infrared spectroscopy (FTIR) analysis was conducted using a Perkin Elmer Spectrum 400 model spectrophotometer to acquire the functional groups of catalysts with wavenumbers ranging from 4000 to 600 cm^{-1}. Surface morphology analysis and quantitative chemical composition analysis of the catalyst were performed using scanning electron microscopy-energy dispersive X-ray (SEM-EDX, Zeiss Evo 50).

Thermogravimetric analysis (TGA-DTG) was carried out using a thermogravimetric analyzer (TGA-50, Shimadzu Corp 00667) to test the catalyst thermal stability from room temperature until 900 °C at 10 °C/min of heating rate with N_2 as the purge gas. Next, the catalysts' crystallinity and structural phase properties were determined by X-ray diffraction (XRD) with PANalytical X'Pert Pro under CuKα (λCu = 0.154056 nm) radiation, whereas the 2θ scanning range was between 20˚ to 90˚. Lastly, the catalyst surface area and porosity were determined using the Brunauer-Emmett-Teller (BET) method (Micromeritics Model ASAP2020).

The photoconversion crude glycerol yield was analyzed using high-performance liquid chromatography (HPLC) (PerkinElmer model). A photodiode-array (PDA) detector was used to detect the chemical compounds in the photocatalytic reaction sample. The reversed phase C18 of the Hypersil 5u ODS 120A model with a 150 mm x 4.60 mm specification was used for the entire analysis. The temperature program was set up from 30 °C to 47 °C with a mobile phase flow rate of 1 mL/min. The mobile phases used were water and acetonitrile (ACN), with a ratio of 90:10, respectively. The analysis time was set at 16 minutes for each sample, while commercial

ethyl acetate and glycerol were used as the standard for calculating the glycerol conversion (%) and product selectivity (%).

Photoconversion of crude glycerol

The crude glycerol was first filtered to remove any particulate matter. Next, the filtered crude glycerol (10 wt%) was prepared by diluting 2 ml of crude glycerol with 20 ml of deionized water. Later, the FTO-PU catalyst foam with 1% FTO was added to the crude glycerol feedstock solution.

The mixture was constantly stirred to ensure complete adsorption on FTO-PU surfaces while being exposed to 30 W of ultraviolet lamp (UV) sources. This experiment was conducted in a black box using a 50 ml beaker with a hot plate, thermometer, magnetic stirrer, and the UV lamp, as illustrated in Figure 1. The experiment was repeated using different reaction parameters: light power (30W, 50W, 70W, 90W, and 120W), reaction time (30 min, 60 min, 90 min, 120 min, and 150 min), crude glycerol concentration (10 wt%, 15 wt%, and 20 wt%), and FTO loading into PU (1%, 2%, and 3%).

Recyclability of the FTO-PU catalyst foam

A recyclability test was conducted to investigate the ability of FTO-PU catalyst foam to be reused. The best performance of FTO-PU in degrading crude glycerol to value-added products was selected for this evaluation after being through all reaction parameters. The recyclability procedure was the same as that in the photocatalysis experiment, except that the test was repeated for six cycles using the same catalyst foam. After the photocatalysis reaction, the foam was filtered out from the products and proceeded with the next cycle without any treatment.

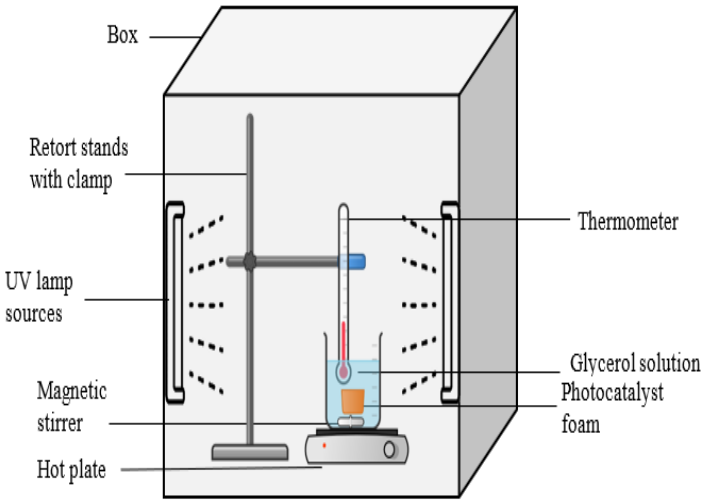

FIGURE 1 Photoconversion experimental setup for transforming crude glycerol into ethyl acetate, conducted in a covered box using a 50 ml beaker, hot plate, thermometer, magnetic stirrer, and the uv lamp

Results and discussion

Catalyst characterization

SEM-EDX for catalyst surface analysis

SEM analysis was conducted to visualize the catalyst surface morphology. The surface morphology of the FTO catalyst was found to be a mixture of various shapes, including irregular structures. Previous studies have stated that the shape of FTO is tetragonal and spherical at 10-20 nm [22,27]. Nonetheless, the tetragonal structure of FTO was further confirmed by XRD (Figure 6). Figure 2 depicts the FTO catalyst's surface morphology image and mapping analysis.

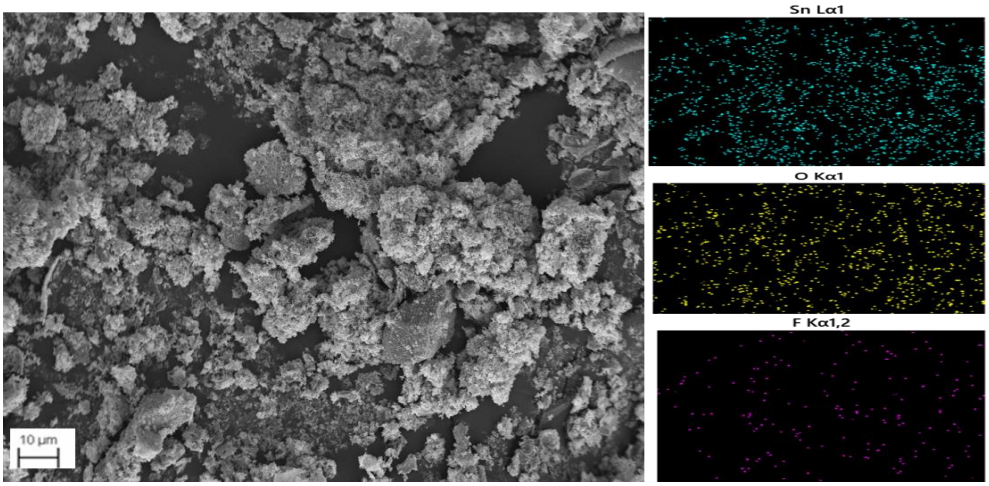

FIGURE 2 Surface morphology and mapping analysis of the FTO catalyst, revealing well-distributed elements of sn, o, and f across the catalyst surface, specifically the fluorine cluster even in trace amounts compared with the other elements

EDX and mapping analyses were conducted to demonstrate the elemental composition and distribution on the catalyst surface. Figure 2 demonstrates well-distributed fluorine clusters even after calcination at high temperatures. Simultaneously, the obtained EDX data revealed all important elemental compositions in FTO, including tin (Sn), oxygen (O), and fluorine (F), as detailed in Table 1.

The atomic percentage of fluorine was relatively low, indicating successful incorporation into the tin oxide network in a small amount. The result was corroborated by XRD analysis, which showed a low peak fluorine intensity (Figure 5). Notably, the use of carbon tape during sample preparation allowed for the detection of carbon elements at a very high atomic percentage [28].

Moreover, the surface morphology analysis of PU foam and FTO-PU foam was performed using high magnification (30 X and 100 X) purposely for easier observation in terms of FTO dispersion, the possible agglomeration into PU foam, and the condition of the pores. Figure 3(a-d) shows images at 30X magnification, while (a′-d′) shows images at 100X magnification respectively. As observed, the PU foam pore surfaces are smooth and flat with tiny, orderly-arranged pores that have also been acknowledged from previous studies [29].

A prominent closed pore type could be determined on the PU foam sample with a diameter ranging from 8 to 35 nm. In addition, the interconnecting surface site between the pores was rougher compared to the FTO-PU foam sample. However, when more FTO is loaded into PU, the interconnecting site surfaces become smoother, and the pores grow irregularly in shape, which is projected to enhance the active catalytic interaction areas. As a result, FTO-PU foam demonstrates better catalytic performance than PU in photoconverting crude glycerol to ethyl acetate. It is worth noting that there is also a significant generation of open pore types on FTO-PU foam for all FTO loading (1, 2, and 3 %), along with the closed pore, which proves that FTO loading could trigger the development of the new open-pore type [30].

Then, concurrently it provides more sites for FTO attachment in the PU foam. In addition, as FTO loading increases, the cavity size of pores decreases, leading to increased strut thickness and improved resistance to deformation [21].

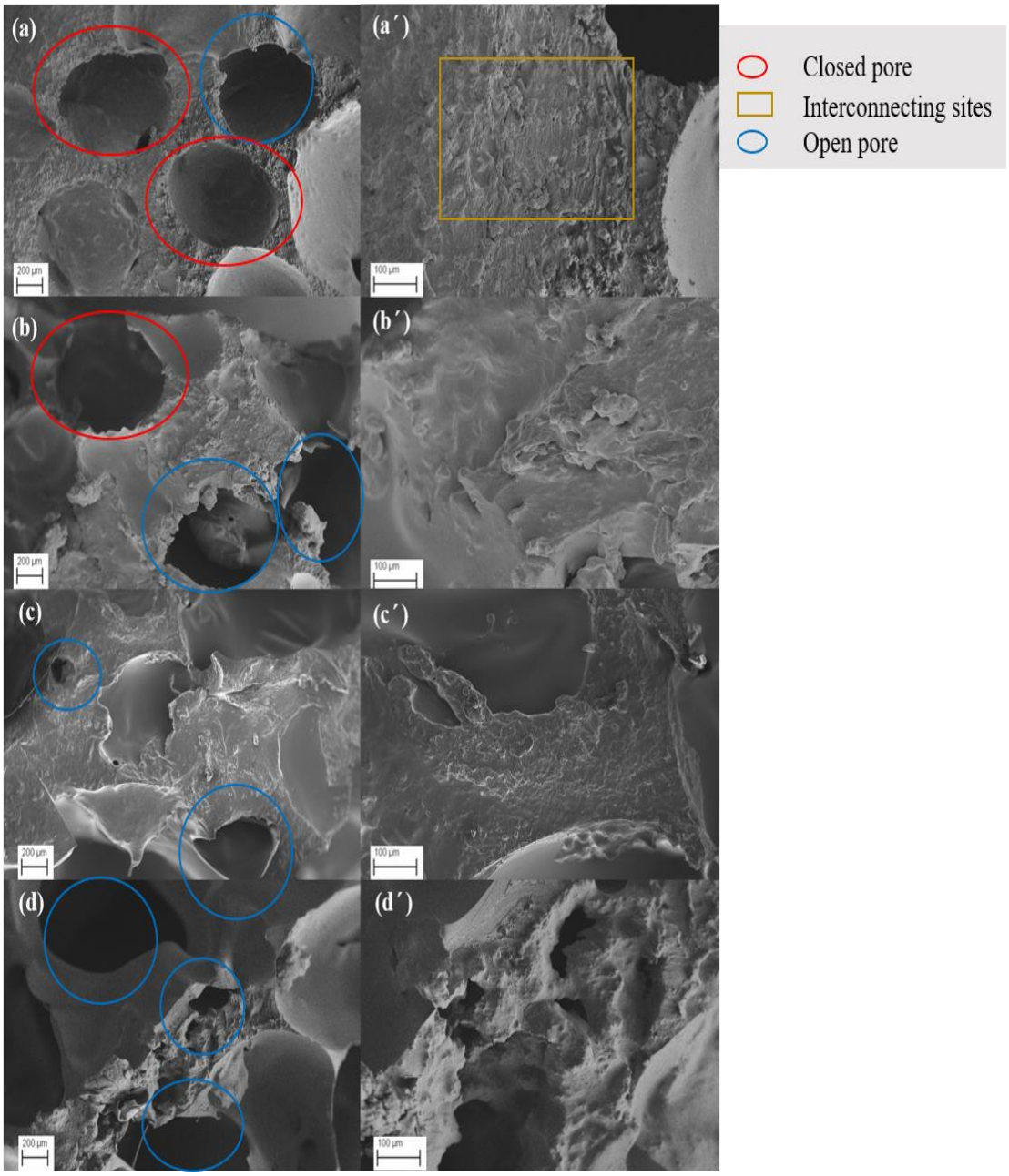

FIGURE 3 Surface morphology of catalyst foam: (a, a´) PU foam, (b, b´) FTO-PU 1%, (c, c´) FTO-PU 2%, and (d, d´) FTO-PU 3%. observations at 30x magnification (a–d) and 100x magnification (a´- d´) reveal the presence of closed pores (red circles) and open pores (blue circles), significantly impacting FTO attachment and the mass transfer process of reactants to the catalyst surface

Thus, the FTO-PU foam is less likely to break apart and melt at high temperatures. However, FTO-PU 1% and FTO-PU 3% showed agglomeration on the PU surface, probably due to the uneven distribution of FTO during the curing process. In contrast, FTO-PU 2% (Figure 3c) exhibited a smoother surface with less obvious agglomeration.

EDX and mapping analysis of the FTO-PU foam (Figure 4) revealed all important elemental compositions in the FTO-PU catalyst foam, including tin (Sn), oxygen (O), carbon (C), and fluorine (F), as indicated in Table 1.

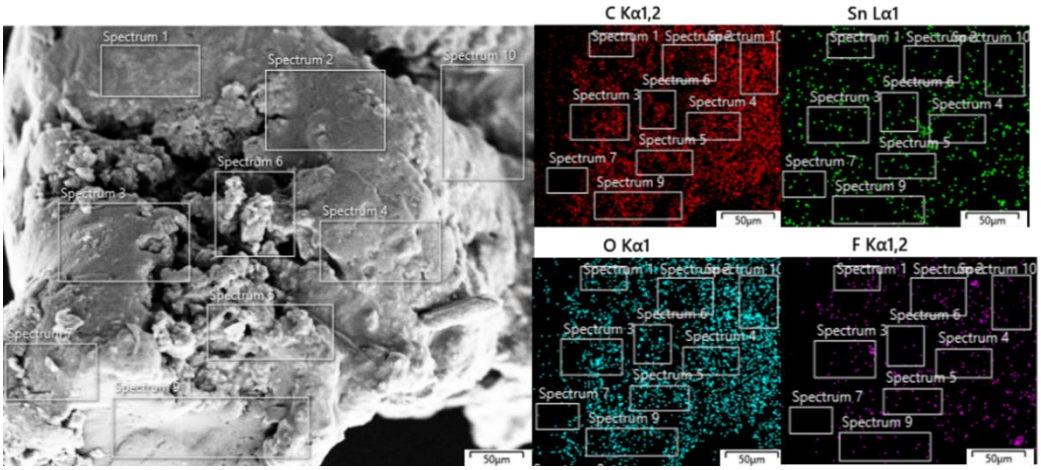

FIGURE 4 Mapping analysis for elements of C, O, F, and Sn detection on FTO-PU 2% catalyst foam

TABLE 1 elemental composition of C, O, Sn, and F in FTO and FTO-PU 2% catalyst foam

Elements	Atomic (%)	
	FTO	FTO-PU 2%
C	33.16	74.90
O	39.08	22.79
F	5.42	1.64
Sn	22.34	0.67

FT-IR for elemental distribution analysis

Next, FTIR analysis was used to identify the functional group of the existing elements in the catalyst. The IR spectra for the comparison of FTO, PU, and FTO-PU foam are shown in Figure 5.

For PU foam, the peak at 3290 cm^{-1} indicates the N-H bond of the amide in urethane. Both peaks at 2854 cm^{-1} and 2927 cm^{-1} are attributed to the -CH_2 stretching bond of the hydrocarbon chain of castor oil and TDI [31]. The three peaks belong to the urethane linkage and indicate the main PU structure. The absorbance peaks appeared at 1711 cm^{-1}, 1602 cm^{-1}, and 1229 cm^{-1}, which were assigned to the carbonyl urethane group (C=O), carbamate (C-NH), and ether (-C-O-C), respectively.

In the case of FTO-PU catalyst foam, the observed peaks are almost similar to those of PU foam due to the low amount of FTO compared to PU. Therefore, important peaks of FTO at 629 cm^{-1} that corresponds to the presence of Sn-O-Sn are not detected in FTO-PU foam as FTO is assumed to be successfully incorporated with PU [32].

A band with peak locations at 3436 cm^{-1} and 1627 cm^{-1} related to FTO was observed in Figure 5(a). The signals were attributed to the stretching and bending vibrations of the O-H bonds associated with water adsorption on the FTO surface [33].

These findings confirmed the chemical bonding between the FTO catalyst and the PU surface.

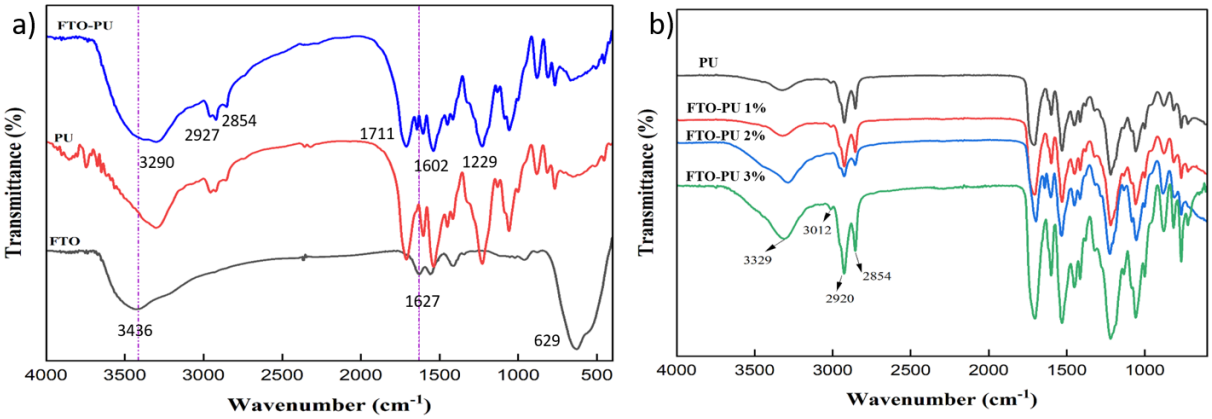

FIGURE 2 Infrared spectra analysis. (a) comparative ir spectra of FTO, FTO-PU 2%, and PU catalyst, highlighting distinct peaks with a purple vertical line denoting features unique to FTO and FTO-PU. (b) varied fto loading in FTO-PU, revealing spectral shifts and intensity changes, elucidating the impact of fto concentration on the material's vibrational characteristics

FTO can also be detected in PU by comparing the spectra for different FTO loadings (Figure 5b). When different FTO loadings are applied to the PU foam, the difference in intensity and frequency of the peak can be seen. FTO-PU 3% has the highest peak intensity. The peaks at 2920 and 2850 cm^{-1} wavelengths, which belonged to the -CH group, were longer, and the peak at 1730 cm^{-1} was more substantial.

FTO-PU 2% shows some shifting of the -NH-stretching bond at a low frequency compared with other foams. The -NH stretching bond shifting in the FTO-PU catalyst foam compared with pure PU provides evidence of -H bond interaction within the functional groups.

XRD for crystallinity and catalyst phase analysis

XRD analysis was used to observe the effect of the intercalation of FTO in PU and the existing chemical phases. Figure 6(a) displays the XRD diffraction patterns for FTO-PU and PU samples. The results indicate that PU was amorphous, while FTO exhibited a crystalline state, which is proven by the crystallinity percentage calculation in Table 2 [26].

The structure and crystallinity of the FTO catalyst were justified by comparison of XRD patterns with the standard JCPDS numbers: SnO_2: 41-1445 and fluorine: 74-6155 [22]. All significant diffraction peaks matched well and exhibited a tetragonal structure of SnO_2. The overlapping of the fluorine phase with SnO_2 explained the effective dispersion of fluorine on the SnO_2 surface, which was attributed to its small size and low concentration [34].

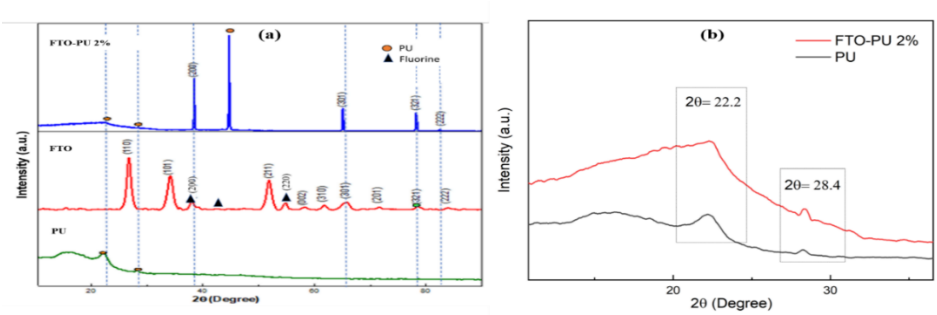

FIGURE 3 X-ray diffraction analysis. (a) Comparative XRD diffractograms featuring FTO-PU 2%, FTO, and PU catalyst, emphasizing shared peaks illustrated by the blue vertical line. (b) Zoomed-in view of the 2θ range 10-40º, focusing on distinctive PU and FTO-PU foam peaks

In addition, the zoomed-in diffractogram between PU and FTO-PU (Figure 6b) shows two significant broad peaks presenting PU foam phases located at 2θ = 22.2˚ and 28.4˚ which can be attributed to scattering from the PU chain with regular interplanar spacing [34]. Previous studies analyzed the crystallinity evidence of PU shown at three peaks in PU: 2θ = 22.2˚, 28.0˚, and 44.0˚ based on the peaks' intensity [36].

Higher intensity indicates higher crystallinity of the PU foam. In this study, an amorphous state in the PU foam was indicated by the low peak intensity observed at 22.2˚ and 28.4˚, with no discernible peak at 44.0˚.

Compared with FTO-PU, a peak at 2θ = 44.6 was observed to have a high intensity that contributed to the changes in crystallinity and can be explained by the degree of cross-linking, which is influenced by the presence of hydroxyl groups in the polyol [37].

FTO loading to the PU foam can interact with the polyol, thus increasing the degree of cross-linking. To sum up, the diffraction peaks at 2θ = 22.0˚, 23.0˚, and 44.6˚ of the FTO-PU foam strongly indicate the existence of the PU phase. Meanwhile, peaks at 38.4˚, 65.1˚, 78.2˚, and 82.4˚ with (200), (321), (321), and (222) lattices correspond to the FTO phase, respectively.

Crystallite size and internal strain were calculated using the Halder–Wagner method for the FTO and FTO-PU catalyst (Table 2). The observations reveal a distinct trend: the introduction of FTO reduces strain, accompanied by a subsequent increase in crystallite size. Upon further incorporation of FTO-PU at 2%, the strain transitions from tensile to compressive. Notably, as the FTO content rises to 3%, the strain reverts to a tensile state, coinciding with an enlargement in crystallite size.

These findings suggest that the lattice strains displayed by the samples are neither uniform nor isotropic [38]. The crystallite size, crystallinity, and strain values are summarised in Table 2.

TABLE 2 Crystallite size, crystallinity, and strain value of fto and fto-pu catalyst foam

Sample	Crystallite size (nm)	Crystallinity (%)	Strain (□ × 10^{-3})
FTO	10.24	90.0	12.94
FTO-PU 1%	21.46	36.2	3.21
FTO-PU 2%	35.36	19.2	2.39
FTO-PU 3%	38.48	22.5	4.02

TGA-DTG for thermal analysis

Next, TGA and DTG analyses were performed on FTO, FTO-PU, and PU catalyst foam to assess thermal stability on degradation. Figure 7 shows that the FTO catalyst had the best thermal stability, with only 21.9% weight loss at 900 °C, assuring that the findings of FTO are bearable at temperatures up to 1200 °C [22].

FTO exhibits one endothermic peak (Figure 7b), which occurs at 250 - 340 °C due to the loss of physically adsorbed water [32]. In PU analysis, there were two stages of thermal deterioration. The first stage was recorded at 250-340 °C with approximately 41% weight loss due to the degradation of the urethane-linkage of isocyanate to form amine derivatives [39].

This stage corresponds to the dissociation of the PU hard section [40]. The second stage of weight loss, between 440 °C and 490 °C, is caused by the dissociation of remaining fragments and the release of CO_2 [35]. Nonetheless, this soft segment breakdown is not very prominent due to the small degradation area, as seen in the graph. Above

490 °C, a constant rate of ratio weight loss was recorded for about 15.01 % until no PU was left at 900 °C. Looking at FTO-PU catalyst foam, the TGA profile looks similar to that of PU foam, but the degradation curve is more distinct. The first stage of FTO-PU's degradation began at a lower temperature, 223 °C, which is not due to low thermal stability but rather due to the removal of low-molecular-weight materials or volatile compounds from the functionalization process of FTO powder supported on PU [40].

FTO-PU ether group decomposition occurred at the same temperature range as PU foam, with 6.11% weight loss. The residue is the weight retained by samples after decomposition at 900 °C. FTO had the highest residue (78.1%), followed by FTO-PU (1.47%), while PU had all its weight decomposed. The 1.47% residue of FTO-PU is deduced as contributed by the amount of FTO immobilization, as FTO has high thermal stability [41].

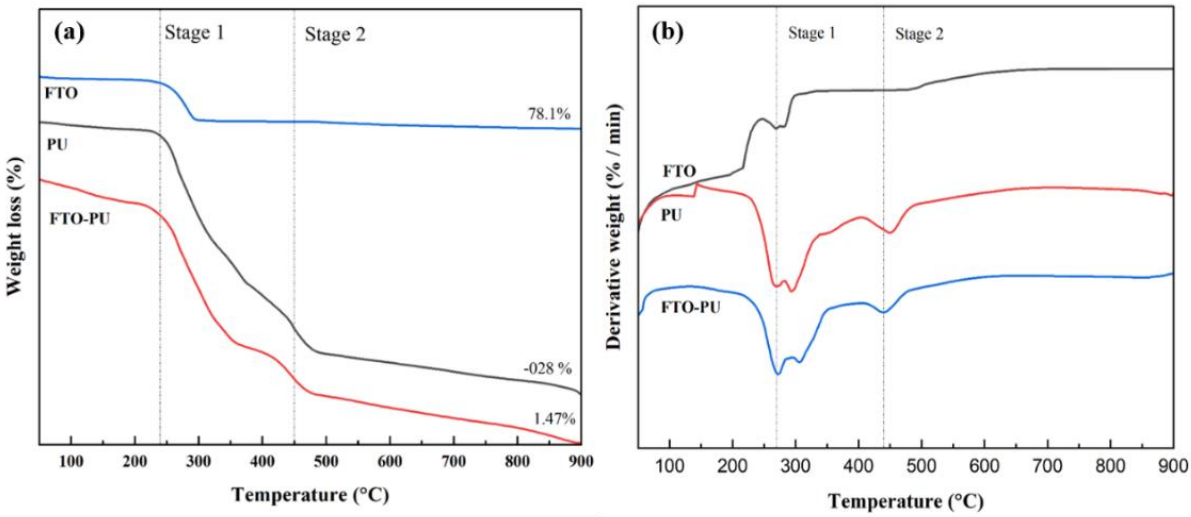

FIGURE 4 Thermogram of FTO, PU, and FTO-PU catalyst foam: (a) TGA and (b) DTG analysis

BET for surface area analysis

Finally, the specific surface area, pore size, and pore volume distribution measured by the BET method in a nitrogen adsorption-desorption environment are summarized in Table 3. The findings show that the FTO catalyst powder had the highest surface area, with 43.14 m^2/g. In general, PU is expected to have a larger surface area since it is a polymer and due to many open pores [39].

Nevertheless, in this study, due to differences in the synthesis process and reagent, the PU's surface area was obtained at 8.49 m^2/g, and it is correlated with closed pore formation, as discussed in the SEM analysis.

When FTO is loaded into PU foam, the surface area decreases compared to FTO on its own, which is suggested to be due to FTO powder blocking the closed pores type in PU foam, resulting in a decrease in the surface area of FTO-PU. When FTO powder was loaded from 1% to 2%, it resulted in a greater surface area (11.128 m^2/g), which proves that FTO successfully bonded and intercalated on the surface of PU foam, and then created a new active site with the development of an open pore type. However, when FTO was loaded up to 3%, the surface area decreased and the pore size increased due to the accumulation of FTO on the PU foam's surface.

SEM analysis strongly supports this finding by showing that PU foam has an uneven surface due to FTO agglomeration onto PU foam [41]. Next, the increase in pore volume and decrease in pore diameter of FTO-PU 1% to 2% evidence a significant amount of FTO can enter PU, thus having a more active site.

The smaller pore diameter can prevent FTO from easily leaching out [22]. Furthermore, the increase in pore volume is also suggested to be due to the widening of existing pores caused by the mechanical stirring effect of FTO during synthesis, which erodes the pores. However, FTO-PU 3% has a lower pore volume, and larger pore size may originate from pores between individual particles aggregated together [42].

TABLE 3 Summary of the surface area, pore volume, and pore size analyzed by the bet method

Sample	S_{ABET} (m^2/g)	V_p (cm^3/g)	D_p (nm)
FTO	43.136	0.0852	7.901
PU	8.494	0.0073	3.471
FTO-PU 1%	5.404	0.0050	3.732
FTO-PU 2%	11.128	0.0084	3.022
FTO-PU 3%	4.168	0.0036	3.452

The average pore diameters of the samples investigated ranged from 3 to 7 nm, indicating that the minerals were mesoporous. According to the International Union of Pure and Applied Chemists (IUPAC definition), microporous materials have a pore diameter of less than 2 nm, mesoporous has a diameter range of 2-50 nm, and macroporous materials have a diameter greater than 50 nm. Therefore, all of the samples investigated were mesoporous materials.

Catalyst performance on photocatalytic activity

This study examined the impact of four reaction parameters on photocatalysis rates, specifically light power, reaction times, FTO loading, and crude glycerol concentration. For supporting purposes, blank experiments were conducted under two conditions to demonstrate that the observed activity resulted from photocatalysis, FTO-PU in the absence of light, and direct photoconversion of crude glycerol without catalyst. The results showed that glycerol conversion was negligible without a catalyst during photoconversion. Ultimately, the primary products obtained in this study were ethyl acetate and ethanol as a minor product.

Figure 8(a) illustrates the remarkable performance of the FTO-PU catalyst in terms of glycerol conversion and ethyl acetate selectivity when subjected to varying light powers (30 W, 50 W, 70 W, 90 W, and 120 W) for 60 min, using a 2% FTO-PU photocatalyst foam. Notably, the catalyst exhibited proficient photocatalytic activity even at a low light power of 30 W. Increasing the light power from 30 W to 70 W resulted in an initial improvement in the conversion and selectivity values. However, at 90 W and 120 W, a decline in conversion, selectivity and yield was observed. Moreover, experiments conducted without the UV radiation displayed significantly lower conversion (40%) and product selectivity (31%), emphasizing the critical role of light power in influencing photocatalytic activity rates. This study supports theories that propose a positive relationship between higher light powers and the formation of electron-hole pairs, thereby hindering recombination.

In contrast, at lower light powers, the separation of electron-hole pairs competes with their recombination, resulting in reduced generation of free radicals and lower conversion of crude glycerol [43]. However, excessive light power can increase the recombination of free charges, leading to the loss of charge carriers [44]. These charge carriers are crucial in production of free radicals that facilitate crude glycerol conversion. The decline in these free radicals at light powers exceeding 70 W reduces crude

glycerol conversion. Therefore, 70 W of light power represents an optimal condition for high crude glycerol conversion (94%) and ethyl acetate selectivity (86%).

Moreover, hypothetically, the reaction duration could impact photocatalytic activity, particularly in terms of crude glycerol adsorption onto the FTO-PU catalyst foam. Theoretically, a longer reaction time allows for a greater conversion rate of crude glycerol, providing more opportunity for the reaction to occur on the catalyst surface and release the desired product. However, the present study observed a decrease in conversion for most reactions when the reaction time was extended from 90 to 150 min (Figure 8b). This decrease is attributed to impurities in the crude glycerol feedstock, which can obstruct the active sites of the FTO-PU catalyst [9].

Prolonged exposure of the FTO-PU catalyst to crude glycerol reduces the available active surface area for free radicals to react with, leading to a lower glycerol conversion rate. This observation aligns with previous research that demonstrated a decline in hydrogen production over time due to catalyst deactivation [45]. Despite decreased crude glycerol conversion over time and light power, the FTO-PU performance maintained ethyl acetate selectivity. The optimal conditions for crude glycerol conversion to ethyl acetate were determined to be a reaction time of 60 min and a light power of 70 W, employing a 2% FTO-PU photocatalyst foam. These parameters yielded high conversion and selectivity percentages, which are in line with theoretical expectations.

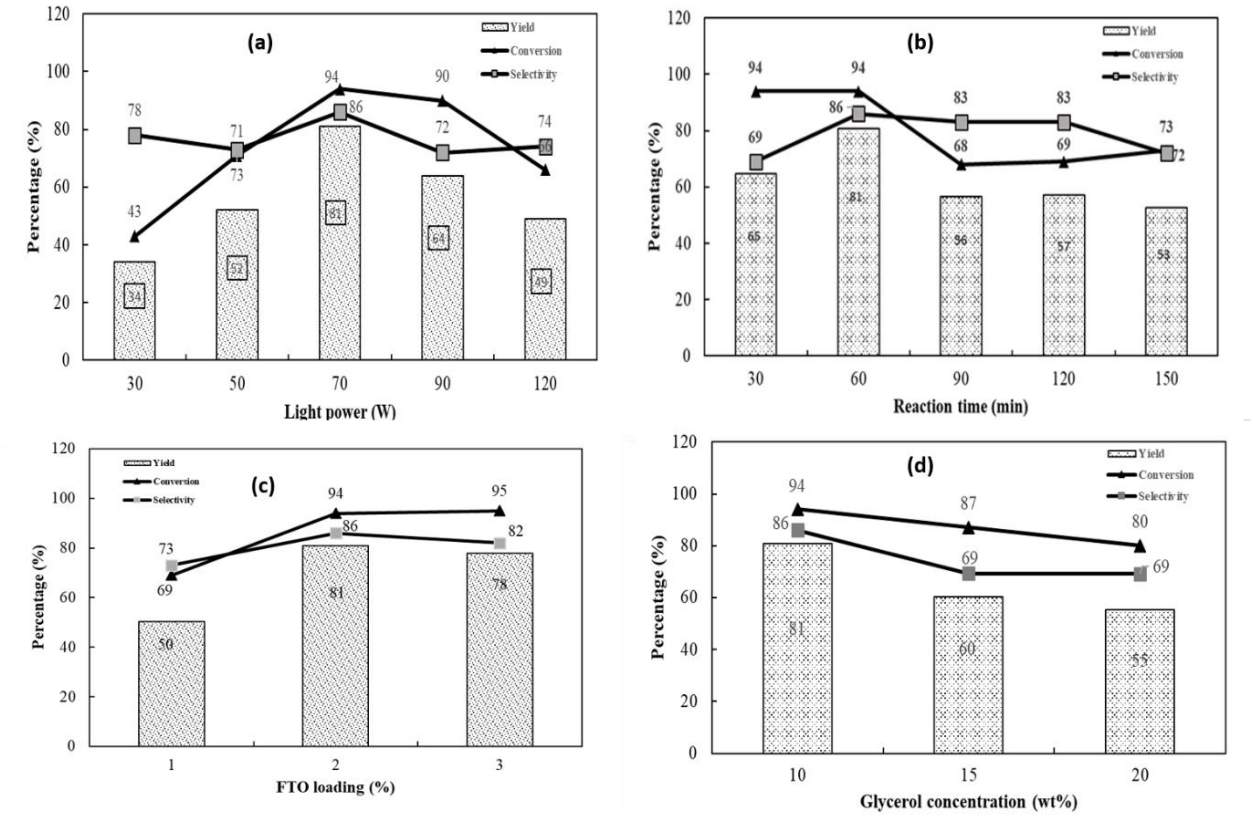

FIGURE 5 Performance of FTO-PU in crude glycerol photoconversion under variable parameters: (a) light power, (b) reaction time. assessment of FTO-PU performance with 70W light intensity and 60 min reaction time across different, and (c) FTO loading and (d) glycerol concentration variations

Next, Figure 8(c) demonstrated the percentage of crude glycerol conversion and ethyl acetate selectivity obtained by utilizing FTO loading on PU at 1%, 2%, and 3% in reactions of 70 W for 60 min. The results demonstrate that FTO-PU 2% provides the highest conversion and selectivity while the values remain stable with FTO-PU 3%. FTO is more stable when the number of acid and basic sites increases. Since the glycerol

conversion process relies on both acid and basic sites, these sites facilitate the cleavage of C-C and C-H bonds, forming a valuable product. Therefore, incorporating higher amounts of FTO into the PU foam enhances the photocatalytic activity by creating more active sites on the catalyst surface to expose additional active sites that can absorb more photons and generate more OH- radicals under irradiation [46].

Consequently, these active sites participate in the photocatalytic reaction, increasing the conversion rates. Thus, the optimal FTO loading for efficient photocatalytic activity was 2% during 70 W reactions lasting for 60 min. This finding is further supported by SEM and BET analysis, which revealed that FTO-PU 2% possessed the highest surface area with minimal agglomeration compared with FTO-PU 1% and 3%. The final reaction parameter of the photoconversion of crude glycerol to ethyl acetate is the feedstock concentration. Essentially, only the crude glycerol that adsorbs onto the surfaces of FTO-PU catalysts will undergo conversion.

The quantity of crude glycerol that adsorbs onto the catalyst surface depends on its initial concentration. In this study, the photocatalytic activity was evaluated using 2% FTO-PU catalysts in combination with various concentrations of crude glycerol under 70 W irradiation for 60 min. The findings demonstrate that the conversion rate decreases as the initial glycerol concentration increases while maintaining a constant amount of catalyst. As the glycerol concentration increases, more organic molecules are adsorbed onto the FTO-PU catalyst until all the active sites are occupied. Consequently, the adsorbed molecules absorb the incident light instead of the FTO-PU catalyst, reducing the number of free radicals reaching the surface [47].

Figure 8(d) presents crude glycerol conversion and ethyl acetate selectivity based on different crude glycerol concentrations. The results align with theoretical expectations, indicating decreased conversion and selectivity percentages with increased feedstock concentration.

Thus, the optimal glycerol concentration for high conversion and selectivity was determined to be 10 wt%. A recyclability test examined the potential for recycling the FTO-PU catalyst under optimized reaction conditions. The experimental procedure involved subjecting the sample to irradiation at 70 W for 60 min using a 2% FTO-PU catalyst and a crude glycerol concentration of 10 wt%. Two approaches were employed to assess the recyclability: washing and without washing the catalyst. Table 4 summarizes the results without catalyst washing. Notably, the treatment of washing the catalyst led to no product formation after the second cycle. This phenomenon is attributed to potential interference with the catalyst's active sites resulting from washing the foam catalyst with ethanol and drying it at 110 ˚C. Therefore, this discovery warrants further investigation and characterization to ascertain the impact of washing on the catalyst's active sites. This study demonstrated that the FTO-PU catalyst possesses moderate recyclability even without desorption.

It is advantageous because it eliminates desorption and saves time. Based on Table 4, a gradual decrease in conversion and selectivity percentages was observed throughout the six cycles, indicating a deterioration in catalyst performance. This decline is likely caused by the adsorption of crude glycerol, which obstructs the active surface area of the FTO-PU catalyst, as evidenced by an increase in the catalyst's weight post-reaction compared with that pre-reaction.

TABLE 4 crude glycerol conversion and ethyl acetate selectivity (%) obtained during six cycles of reaction

Cycles	Conversion (%)	Ethyl acetate selectivity (%)	Yield (%)
C1	94	86	80.8
C2	69	67	46.2
C3	45	65	29.3
C4	21	65	13.7
C5	51	29	14.8
C6	37	33	12.2

To assess the stability of the catalysts under photocatalysis conditions, the surface morphology, catalyst composition, and porosity were examined using XRD, SEM, and BET analysis. Figure 9 illustrates the XRD spectra that reveal only the PU characteristics in the first and sixth cycles, as described in Figure 6. However, all peaks indicating FTO and PU crystallinity disappeared after subsequent cycles, indicating decreased FTO-PU performance upon recycling, highlighting the significance of FTO properties in achieving high conversion rates and selectivity. The absence of the FTO peak in the XRD diffractogram is attributed to the previous presence of feedstock, which obstructed the detection of FTO particles. This phenomenon occurs due to catalyst deactivation factors, namely fouling and coking formation. Fouling refers to the physical deposition of species from the fluid phase onto the catalyst surface, leading to activity loss due to active sites and pores blockage. Coking involves a chemisorption reaction where carbon completely encapsulates a metal particle, resulting in its complete deactivation [48].

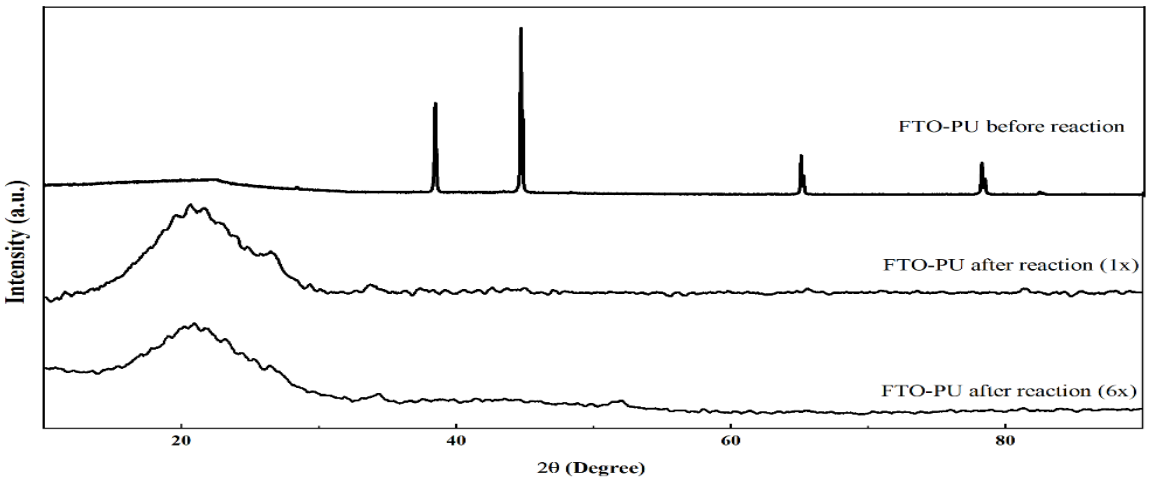

FIGURE 6 Comparison of the XRD diffractogram for the FTO-PU 2% catalyst before and after the reaction

As depicted in Figure 10 through the SEM image, the FTO-PU catalyst after the first reaction (Figure 10b) exhibits reduced porosity and increased agglomeration on its surface due to the attached crude glycerol. However, the sixth post-reaction FTO-PU catalyst (Figure 10c) displayed a larger pore size, which correlates with the BET analysis (Table 5), showing increased porosity and surface area. Previous research has demonstrated that catalyst deactivation caused by sintering can increase the surface area and porosity, mainly when the reaction is structure-sensitive as the crystallite size increases [49].

Nevertheless, since this study did not involve a sintering process, the XRD calculation (Table 5) revealed an increase in the crystallite size for the sixth post-reaction catalyst compared with the first post-reaction catalyst.

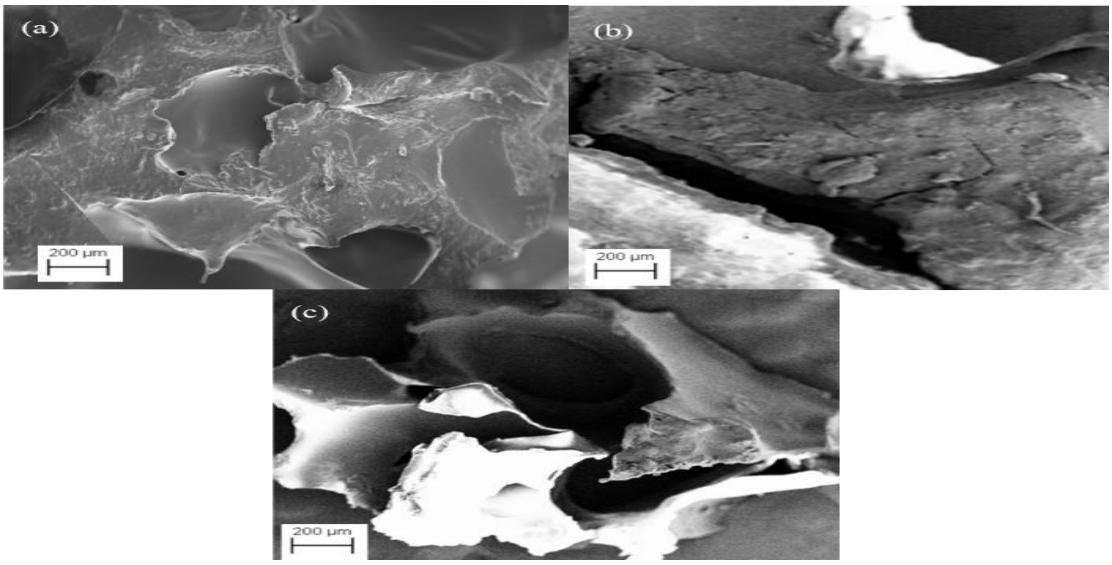

FIGURE 10 sem image of fto pu catalyst: (a) before reaction, (b) after 1st reaction, and (c) after 6th reaction

Table 5 the comparison of surface area by the bet method and crystallite size from XRD calculation for pre-reaction and post-reaction catalysts

Sample	S_{ABET} (m^2/g)	Crystallite size (nm)
FTO-PU 2% (before reaction)	11.128	27.78
FTO-PU 2% (after 1st reaction)	3.832	18.97
FTO-PU 2% (after 6th reaction)	17.613	70.01

This discovery unveils a new finding that necessitates further investigation, as crystallite size can change without sintering. Despite the larger pore size and higher surface area observed in the sixth post-reaction catalyst, its recyclability did not improve, as evidenced by the blocking of FTO based on the XRD spectra. Moreover, relatively large pores can lead to significant coke formation and enhance the reaction rate by improving diffusion efficiency [50].

The large pore size in this study contributed to coke formation, resulting in low conversion and selectivity. Therefore, these factors confirm that the appropriate and optimal pore size and surface area are crucial for good catalytic performance in high conversion and selectivity. Despite this, the FTO-PU foam maintained a significant level of crude glycerol conversion and ethyl acetate selectivity even after the sixth cycle.

Conclusion

This study synthesized a novel photocatalyst FTO-PU foam by immobilizing FTO powder onto PU foams. The resulting FTO-PU foam displayed a stable structure that resisted breaking, and FTO did not easily leach out of the foam. SEM, EDX, and XRD.
characterizations confirmed good dispersion of FTO in the matrix and on the PU foam surface. However, most characterizations

followed PU characteristics due to the low amount of loaded FTO, confirmed by FT-IR and TGA analyses, revealing PU properties in functional groups and thermal stability. FTO-PU foam was expected to have a larger surface area than the FTO catalyst.

Still, BET analysis showed a lower surface area than the FTO catalyst because FTO blocked the PU foam pores and immersed in the intrinsic PU pores, reducing the FTO-PU surface area. Despite the lower surface area, the synthesized FTO-PU achieved high crude glycerol conversion (94%) and ethyl acetate selectivity (86%), yielding an 81% overall yield with optimal parameters of 70 W of light power for 60 min with a 10 wt% concentration of crude glycerol using the FTO-PU 2% foam. One advantage of the FTO-PU catalyst foam for converting crude glycerol to ethyl acetate is its high selectivity, and ethyl acetate remained stable without reversible reactions to other products. Furthermore, the novel photocatalyst could be used six times without desorption and washing while maintaining a significant percentage value for crude glycerol conversion and ethyl acetate selectivity, demonstrating the potential application value of FTO-PU as an innovative platform for effective biomass conversion into value-added chemicals. Future research in photocatalysis and biomass conversion should focus on enhancing the stability and recyclability of FTO-PU, addressing crystallinity issues through alternative formulations and reagents. In addition, a deeper understanding of catalytic mechanisms, achieved through techniques like temperature-programmed reduction (TPR), temperature-programmed desorption (TPD), and density functional theory (DFT) calculations, and quantifying hydroxyl radical production, is crucial for refining catalytic systems. These research directions are essential for meeting the growing demand for cleaner industrial processes and eco-friendly sources of chemicals and fuels, contributing to a greener and more sustainable future for the chemical and energy sectors.

Acknowledgments

The authors would like to acknowledge funding from the Ministry of Higher Education of Malaysia, with grant number 600-ITMI/FRGS 5/3 (403/2019). The authors declare that they have no conflict of interest.

Funding

The authors would like to thank the Faculty of Applied Sciences, University Technology MARA for providing instrumentation facilities for conducting research.

Authors' Contributions

Sadina Shazwani conceptualized the work performed, the investigations, and the writing – the original draft. Wan Zurina played a significant role in the study's conception, contributed to data interpretation, and was actively involved in revising the manuscript for intellectual content. Noraini and Norazizi provided resources and supervision.

Conflicts of Interest

The authors declare that they have no conflict of interest in this article.

Orcid:

Noraini Hamzah:
https://www.orcid.org/0000-0001-7885-4098
Norazzizi Nordin:
https://www.orcid.org/0000-0003-0147-6097
Wan Zurina Samad:
https://www.orcid.org/0009-0008-3232-0849

References

[1] B. Dudley, BP statistical review of world energy, *Energy economic, Centre for energy economics research and policy. British Petroleum, Available via https://www. bp. com/en/global/corporate/energy-*

economics/statistical-review-of-world-energy/electricity. html, *5*, **2018**. [Google Scholar], [Publisher]

[2] J.L. Holechek, H.M.E. Geli, M.N. Sawalhah, R. Valdez, A Global Assessment: Can Renewable Energy Replace Fossil Fuels by 2050? *Sustainability* (Switzerland), **2022**, *14,* 4792 [Crossref], [Google Scholar], [Publisher]

[3] P.A. Owusu, S. Asumadu-Sarkodie, A review of renewable energy sources, sustainability issues and climate change mitigation, *Cogent Engineering,* **2016**, *3*, 1167990. [Crossref], [Google Scholar], [Publisher]

[4] C.R. Chilakamarry, A.M. Sakinah, A.W. Zularisam and A. Pandey, Glycerol waste to value added products and its potential applications, *Systems Microbiology and Biomanufacturing*, **2021**, *1*, 378–396. [Crossref], [Google Scholar], [Publisher]

[5] C.C. Chong, A. Aqsha, M. Ayoub, M. Sajid, A. Z. Abdullah, S. Yusup, B. Abdullah, A review over the role of catalysts for selective short-chain polyglycerol production from biodiesel derived waste glycerol, *Environmental Technology & Innovation*, **2020**, *19*, 100859. [Crossref], [Google Scholar], [Publisher]

[6] S. Konstantinovic, B. Danilovic, J. Ciric, S. Ilic, D. Savic, V. Veljkovic, Valorization of crude glycerol from biodiesel production, *Chemical Industry and Chemical Engineering Quarterly* **2016**, *22* 461–489. [Crossref], [Google Scholar], [Publisher]

[7] S. Nomanbhay, R. Hussein, M.Y. Ong, Sustainability of biodiesel production in Malaysia by production of bio-oil from crude glycerol using microwave pyrolysis: a review, *Green Chemistry Letters and Reviews*, **2018**, *11*, 135–157. [Crossref], [Google Scholar], [Publisher]

[8] U.I. Nda-Umar, I. Ramli, Y.H. Taufiq-Yap, E.N. Muhamad, An overview of recent research in the conversion of glycerol into biofuels, fuel additives and other bio-based chemicals, *Catalysts*, **2019**, *9*, 15 [Crossref], [Google Scholar], [Publisher]

[9] M.N. Gatti, J.L. Cerioni, F. Pompeo, G.F. Santori, N.N. Nichio, High yield to 1-propanol from crude glycerol using two reaction steps with ni catalysts, *Catalysts*, **2020**, *10*, 615. [Crossref], [Google Scholar], [Publisher]

[10] P.S. Kong, M.K. Aroua, W.M. Daud, Conversion of crude and pure glycerol into derivatives: A feasibility evaluation, *Renewable and Sustainable Energy Reviews,* **2016**, *63*, 533–555. [Crossref], [Google Scholar], [Publisher]

[11] J. Kaur, A.K. Sarma, M.K. Jha, P. Gera, Valorisation of crude glycerol to value-added products: Perspectives of process technology, economics and environmental issues, *Biotechnology Reports*, **2020**, *27*. [Crossref], [Google Scholar], [Publisher]

[12] I.C. Freitas, R.L. Manfro, M.M.V.M. Souz, Hydrogenolysis of glycerol to propylene glycol in continuous system without hydrogen addition over Cu-Ni catalysts, *Applied Catalysis B: Environmental,* **2018**, *220*, 31–41. [Crossref], [Google Scholar], [Publisher]

[13] V. K. Garlapati, U. Shankar, A. Budhiraja, Bioconversion technologies of crude glycerol to value added industrial products, *Biotechnology Reports,* **2016**, *9,* 9–14. Crossref], [Google Scholar], [Publisher]

[14] O. Monfort, Y. Wu, Photocatalytic Processes for Environmental Applications, *Processes*, **2021**, *9*, 2080. [Crossref], [Google Scholar], [Publisher]

[15] L.I. Granone, F. Sieland, N. Zheng, R. Dillert, D.W. Bahnemann, Photocatalytic conversion of biomass into valuable products: a meaningful approach?, *Green chemistry,* **2018**, *20*, 1169-1192. [Crossref], [Google Scholar], [Publisher]

[16] R. Chong, J. Li, X. Zhou, Y. Ma, J. Yang, L. Huang, H. Han, F. Zhang, C. Li, Selective photocatalytic conversion of glycerol to hydroxyacetaldehyde in aqueous solution on facet tuned TiO 2-based catalysts, *Chemical communications,* **2014**, *50*, 165–167. [Crossref], [Google Scholar], [Publisher]

[17] J. Yu, F. Dappozze, J. Martín-Gomez, J. Hidalgo-Carrillo, A. Marinas, P. Vernoux, A. Caravaca, C. Guillard, Glyceraldehyde production by photocatalytic oxidation of glycerol on WO3-based materials, *Applied Catalysis B: Environmental,* **2021**, *299*, 120616. [Crossref], [Google Scholar], [Publisher]

[18] T. Yamamoto, H. Mine, S. Katada, T. Tone, Direct ethyl acetate synthesis from ethanol over amorphous-, monoclinic-, tetragonal ZrO2 supported copper catalysts prepared from the same zirconium source, *Applied Catalysis B: Environmental*, **2023**, *327*, 122433. [Crossref], [Google Scholar], [Publisher]

[19] Y. Chen, Q. Zhang, K. Liu, S. Zhang, X. Zhang, H. Liu, Simulation, optimization and intensification of the process for co-production of ethyl acetate and amyl acetate by reactive distillation, *Process Safety and Environmental Protection*, **2023**, *171*, 607-618. [Crossref], [Google Scholar], [Publisher]

[20] W. Piotrowski, R. Kubica, Integration of the process for production of ethyl acetate by an enhanced extraction process, *Processes*, **2021**, *9,* 1425. [Crossref], [Google Scholar], [Publisher]

[21] W.Z. Samad, W.N. Roslam, W. Isahak, N. Nordin, M.A. Yarmo, M.R. Yusop, Gylcerol conversion over novel fluorine-doped tin oxide supported catalyst: effect of metal loadings and glycerol concentration, *Malaysian Journal of Analytical Sciences*, **2015**, *19*, 55-64. [Google Scholar], [Publisher]

[22] W.Z. Samad, M. Goto, H. Kanda, Wahyudiono, N. Nordin, K.H. Liew, M.A. Yarmo, M.R. Yusop, Fluorine-doped tin oxide catalyst for glycerol conversion to methanol in sub-critical water, *J, Supercrit. Fluids*, **2017**, *120*, 366–378. [Crossref], [Google Scholar], [Publisher]

[23] F.V. Amorim, R.J.R. Padilha, G.M. Vinhas, M.R. Luiz, N.C. de Souza and Y.M.B. de Almeida, Development of hydrophobic polyurethane/castor oil biocomposites with agroindustrial residues for sorption of oils and organic solvents, *J, Colloid Interface Sci*, **2021**, *581*, 442–454. [Crossref], [Google Scholar], [Publisher]

[24] M. Anju, N.K. Renuka, Magnetically actuated graphene coated polyurethane foam as potential sorbent for oils and organics, *Arabian Journal of Chemistry,* **2020**, *13*, 1752–1762. [Crossref], [Google Scholar], [Publisher]

[25] D.S. Pattanayak, J. Mishra, J. Nanda, P.K. Sahoo, R. Kumar, N.K. Sahoo, Photocatalytic degradation of cyanide using polyurethane foam immobilized Fe-TCPP-S-TiO_2-rGO nano-composite, *Journal of Environmental Management,* **2021**, *297*, 113312. [Crossref], [Google Scholar], [Publisher]

[26] H. Peng, T. Romero, P. Bertani, V. Ritleng, Polydopamine-Coated Polyurethane Foam as a Structured Support for the Development of an Easily Reusable Heterogeneous Photocatalyst Based on Eosin Y. *Catalysts,* **2023**, *13*, 589. [Crossref], [Google Scholar], [Publisher]

[27] L. Xiao, R. Liao, S. Yang, Y. Qiu, M. Wang, Z. Zhang, J. Du, Z. Xie, Facile Fabrication of F-Doped SnO_2 Nanomaterials for Improved Photocatalytic Activity. *Coatings,* **2022**, *12*, 795. [Crossref], [Google Scholar], [Publisher]

[28] O.F. Olorundare, T.A.M. Msagati, R.W.M. Krause, J.O. Okonkwo, B.B. Mamba, Polyurethane composite adsorbent using solid phase extraction method for preconcentration of metal ion from aqueous solution, *International Journal of Environmental Science and Technology,* **2015**, *12*, 2389–2400. [Crossref], [Google Scholar], [Publisher]

[29] M.R. Lubis, R. Saputra, M.D. Alfarabi, S. Sarah, May. Characterization of modified polyurethane foam adsorbents for mercury adsorption applications, In *IOP Conference Series: Materials Science and Engineering,* **2022**, *845*, 12002. [Crossref], [Google Scholar], [Publisher]

[30] G. Sung, J.S. Kim, J.H. Kim, Sound absorption behavior of flexible polyurethane

foams including high molecular-weight copolymer polyol, *Polymers for Advanced Technologies*, **2017**, *29*, 852–859. [Crossref], [Google Scholar], [Publisher]

[31] A.D. Macalino, V.A. Salen, L.Q. Reyes, September. Castor oil based polyurethanes: synthesis and characterization. *In IOP Conference Series: Materials Science and Engineering, IOP Publishing*, **2017**, *229*, 12016. [Crossref], [Google Scholar], [Publisher]

[32] H. Yang, C. Li, A. Tang, Synthesis and Characterization of Fluorine-Doped Tin Dioxide Nanocomposites, In *Proceedings of the 8 th Pacific Rim International Congress on Advanced Materials and Processing*, **2013**, 1507–1514. [Crossref], [Google Scholar], [Publisher]

[33] M. Kardeş, H.C. Yatmaz, K. Öztürk, ZnO Nanorods Grown on Flexible Polyurethane Foam Surfaces for Photocatalytic Azo Dye Treatment, *ACS Applied Nano Materials,* **2023** *6*, 6605–6613. [Crossref], [Google Scholar], [Publisher]

[34] S.Y. Mak, K.H. Liew, C.C. Chua, M.A. Yarmo, B.H. Yahaya, W.Z. Samad, M.S.M. Jamil, R.M. Yusop, Palladium nanoparticles supported on fluorine-doped tin oxide as an efficient heterogeneous catalyst for Suzuki coupling and 4-nitrophenol reduction, *Journal of Chemical Sciences*, 2019, *131*, 1-12. [Crossref], [Google Scholar], [Publisher]

[35] G. Trovati, E.A. Sanches, S.C. Neto, Y.P. Mascarenhas, G.O. Chierice, Characterization of polyurethane resins by FTIR, TGA, and XRD, *Journal of Applied Polymer Science*, **2010**, *115*, 263–268. [Crossref], [Google Scholar], [Publisher]

[36] M.S.J. Khan, T. Kamal, F. Ali, A.M. Asiri, S.B. Khan, Chitosan-coated polyurethane sponge supported metal nanoparticles for catalytic reduction of organic pollutants, *International journal of biological macromolecules*, **2019**, *132*, 772–783. [Crossref], [Google Scholar], [Publisher]

[37] M.M. Ghobashy, Z.I. Abdeen, Radiation crosslinking of polyurethanes: characterization by FTIR, TGA, SEM, XRD, and raman spectroscopy, *Journal of Polymers,* **2016**, 1–9. [Crossref], [Google Scholar], [Publisher]

[38] L. Motevalizadeh, M. Tahani, A Phenomenological Study of Chromium Impurity Effects on Lattice Microstrains of SnO2 Nanoparticles Prepared Using Sol–Gel Technique, *Crystals*, **2023**, *13*, 919. [Crossref], [Google Scholar], [Publisher]

[39] M.E. Bourain, A. Abdelghany, Sorption Features of Polyurethane Foam Functionalized with Salicylate for Chlorpyrifos: Equilibrium, Kinetic Models and Thermodynamic Studies, *Polymers*, **2020**, *12*, 2036. [Crossref], [Google Scholar], [Publisher]

[40] L. Stroea, A.L. Chibac-Scutaru, V. Melinte, Aliphatic polyurethane elastomers quaternized with silane-functionalized TiO2 nanoparticles with UV-shielding features, *Polymers*, **2021**, *13*, 1318. [Crossref], [Google Scholar], [Publisher]

[41] A. Ahmad, S.A.M. Jamil, T. Shean, Y. Choong, A.H. Abdullah, M.S. Mastuli, N. Othman, N. Jiman, Green flexible polyurethane foam as a potent support for Fe-Si adsorbent, *Polymers,* **2019**, *11*, 2011. [Crossref], [Google Scholar], [Publisher]

[42] M.A. Islam, Competitive sorption of metal ions and humic acid onto manganese oxides and boehmite, *La Trobe University, Australia*, **2018**. [Google Scholar], [Publisher]

[43] K.M. Reza, A. Kurny, F. Parameters affecting the photocatalytic degradation of dyes using TiO 2: a review, *Applied Water Science,* **2017**, *7*, 1569–1578. [Crossref], [Google Scholar], [Publisher]

[44] L. Zhu, M. Zhang, J. Xu, C. Li, J. Yan, G. Zhou, W. Zhong, T. Hao, J. Song, X. Xue, Z. Zhou, R. Zeng, H. Zhu, C.C. Chen, R.C.I. Chen, Y. Zou, J. Nelson, Y. Zhang, Y. Sun, F. Liu, Single-junction organic solar cells with over 19% efficiency enabled by a refined double-fibril network morphology, *Nature Materials,* **2022**, *21*, 656–663. [Crossref], [Google Scholar], [Publisher]

[45] M.R. Karimi Estahbanati, M. Feilizadeh, F. Attar, M.C. Iliuta, Current developments and future trends in photocatalytic glycerol valorization: process analysis, *Reaction Chemistry & Engineering*, **2021**, *6*, 197–219. [Crossref], [Google Scholar], [Publisher]

[46] R. Gusain, N. Kumar, S.S. Ray, Factors influencing the photocatalytic activity of photocatalysts in wastewater treatment. *Photocatalysts in Advanced Oxidation Processes for Wastewater Treatment*, **2020**, 229-270. [Crossref], [Google Scholar], [Publisher]

[47] S. Zhang, P. Gu, R. Ma, C. Luo, T. Wen, G. Zhao, W. Cheng, X. Wang, Recent developments in fabrication and structure regulation of visible-light-driven g-C3N4-based photocatalysts towards water purification: a critical review, *Catalysis Today*, **2019**, *335*, 65–77. [Crossref], [Google Scholar], [Publisher]

[48] M.D. Argyle, C.H. Bartholomew, Heterogeneous catalyst deactivation and regeneration: a review, *Catalysts*, **2015**, *5*, 145-269. [Crossref], [Google Scholar], [Publisher]

[49] M.D. Nasrallah, Sintering process and catalysis, *Int J Nanomater Nanotechnol Nanomed*, **2018**, *4*, 1–3. [Crossref], [Google Scholar], [Publisher]

[50] H. Yang, T. Han, W. Yang, L. Sandström, P. G. Jönsson, Influence of the porosity and acidic properties of aluminosilicate catalysts on coke formation during the catalytic pyrolysis of lignin, *Journal of Analytical and Applied Pyrolysis*, **2022**, *165*, 105536. [Crossref], [Google Scholar], [Publisher]

How to cite this article: Sadina Shazwani Mastika*, Noraini Hamzah, Norazzizi Nordin, Wan Zurina Samad, High-performance of fluorine-doped tin oxide immobilized on polyurethane foam composite for crude glycerol to ethyl acetate photoconversion. . *Journal of Medicinal and Pharmaceutical Chemistry Research*, 2024, 6(5), 581-602. **Link:** http://jmpcr.samipubco.com/article_187638.html